Special Collection

Decoration of Squalenoyl-Gemcitabine Nanoparticles with Squalenyl-Hydroxybisphosphonate for the Treatment of Bone Tumors

Carlos Rodríguez-Nogales,[a] Didier Desmaële,[b] Víctor Sebastián,[c] Patrick Couvreur,*[b] and María J. Blanco-Prieto*[a]

Therapeutic perspectives of bone tumors such as osteosarcoma remain restricted due to the inefficacy of current treatments. We propose here the construction of a novel anticancer squalene-based nanomedicine with bone affinity and retention capacity. A squalenyl-hydroxybisphosphonate molecule was synthetized by chemical conjugation of a 1-hydroxyl-1,1-bisphosphonate moiety to the squalene chain. This amphiphilic compound was inserted onto squalenoyl-gemcitabine nanoparticles using the nanoprecipitation method. The co-assembly led to nanoconstructs of 75 nm, with different morphology and colloidal properties. The presence of squalenyl-hydroxybisphosphonate enhanced the nanoparticles binding affinity for hydroxyapatite, a mineral present in the bone. Moreover, the *in vitro* anticancer activity was preserved when tested in commercial and patient-treated derived pediatric osteosarcoma cells. Further *in vivo* studies will shed light on the potential of these nanomedicines for the treatment of bone sarcomas.

Introduction

Osteosarcoma (OS) is the most common primary osseous tumor. Its age-specific incidence follows a bimodal distribution peak as it occurs mostly during the second decade of life, and to a lesser extent in patients over 50 years-old.[1,2] The complex biology of this cancer is associated with a progression and a fatal outcome, and it has survival rates of 17–34% in high-risk patients.[3,4] For this reason, pre-adjuvant and adjuvant chemotherapy have become indispensable for successful surgical resection of the primary tumor and prevention of future relapses and metastases.[5,6] Nevertheless, the aggressiveness of these tumors obliges oncologists to administer high doses of cytostatic agents, which in many cases trigger limiting adverse effects, treatment abandonment or failure.[7]

On November 17, 2020, we celebrated 25 years of cancer nanomedicine following the market approval of Doxil® (liposomal-doxorubicin) for the treatment of AIDS-related Kaposi's sarcoma.[8] Thereafter, around 15 anticancer nanomedicines have been commercialized so far with the aim of ameliorating the therapeutic index of chemotherapeutic drugs.[9,10] Some of the potential benefits reported about the administration of these nanosized *(i.e.,* 1–1000 nanometers) drug delivery systems rely on passive or active tumor-targeting abilities. Passive targeting is mainly associated with the well-described enhanced permeation and retention effect of nanoparticles (NPs) around the tumor microenvironment.[11] Conversely, active targeting can be mediated by the conjugation of specific ligands or antibodies among other moieties to their surface.[12] This second strategy led researchers to identify, in case of OS, structural chemical elements that preferentially bind to the hydroxyapatite (HA) mineral present in the bone. Among these, 1-hydroxy-1,1-bisphosphonate derivatives showed considerable efficacy as bone-targeting ligands.[13,14] These are analogs of pyrophosphates able to bind irreversibly to calcium ions present in the HA. In fact, bisphosphonates are usually the first choice for osteoporosis treatment since they inhibit bone resorption mediated by osteoclasts.[15,16]

Recently, several studies have described the use of bisphosphonates to construct bone-targeted nanomedicines.[17] Many of them report the attachment of the commercially available molecule of alendronate or zolendronate to the surface of polymer NPs via various linkers.[18] However, classic polymer nanoformulations often display low encapsulation rates together with an uncontrolled burst release behavior that limit treatment efficacy. By using the so-called "squalenoylation" technology, drugs can be chemically modified into biocompat-

[a] *Dr. C. Rodríguez-Nogales, Dr. M. J. Blanco-Prieto*
Chemistry and Pharmaceutical Technology
Faculty of Pharmacy,
Universidad de Navarra-IdisNA
Irunlarrea 1, 31008 Pamplona (Spain)
E-mail: mjblanco@unav.es
[b] *Dr. D. Desmaële, Prof. P. Couvreur*
Institut Galien Paris-Sud UMR CNRS 8612
Université Paris-Saclay
Jean Baptiste Clément 5, 92290 Châtenay-Malabry Cedex (France)
E-mail: patrick.couvreur@universite-paris-saclay.fr
[c] *Dr. V. Sebastián*
Instituto de Nanociencia y Materiales de Aragón (INMA)
CSIC-Universidad de Zaragoza
Mariano Esquillor López, 50008 Zaragoza (Spain)

Supporting information for this article is available on the WWW under https://doi.org/10.1002/cmdc.202100464

This article belongs to the Special Collection "Nanomedicine: Drug Delivery and Nanodrugs".

ible amphiphilic prodrugs by linkage with the squalene, a natural and endogenous lipid.[19] These squalenoyl bioconjugates are able to form spontaneously drug-based NPs in a very easy nanoprecipitation process that does not require surfactants, phospholipids or polymers. This concept can be upgraded for a wide variety of drugs and allows for very high encapsulation rates with no burst release.[20] The cytostatic agent chosen for this study was the nucleoside analog gemcitabine (dFdC), prescribed as a second line treatment for OS. The improved anticancer efficacy of the squalenoyl-gemcitabine (dFdC–Sq) nanomedicine is now well established in many *in vivo* preclinical models, comparatively to dFdC free.[21,22] As a follow-up of our previous papers, we now propose that the chemical binding of squalene to a 1-hydroxy-1,1-bisphosphonic acid head group might deliver a self-assembling compound embedding a bone mineral targeting moiety. This approach was conceived to achieve a prolonged and selective anticancer activity in the bone tumor area, avoiding systemic toxicities. Thus, squalenyl hydroxybisphosphonic acid (HbisP–Sq) and dFdC–Sq were hypothesized to perform a novel multidrug co-assembly aiming at the construction of a bone-targeted nanomedicine. This study reports the design and physicochemical characterization of dFdC–Sq | HbisP–Sq NPs. To this end, we performed the chemical synthesis of a squalenyl bisphosphonic acid derivative. HbisP–Sq, dFdC–Sq and dFdC–Sq | HbisP–Sq NPs were formulated using the nanoprecipitation method. Their binding affinity to HA crystals was evaluated by spectrofluorimetry and confocal microscopy and *in vitro* experiments were performed using pediatric OS cells. Thus, dFdC–Sq NPs decorated with a bone mineral targeting bisphosphonate moiety (HbisP–Sq) were successfully developed.

Results and Discussion

Chemistry of HbisP-Sq 4

At the outset of the study, the covalent coupling of alendronate to squalene was explored. The coupling of fatty acids with alendronate has been previously reported using standard DCC/NHS chemistry.[23] Unfortunately, 1,1′,2-trisnorsqualenic acid (**1**) obtained in a few steps from squalene[24] failed to deliver the desired coupling product in the same conditions. The main hurdle in the process appeared to be the extreme lipophilicity of the squalenic acid, which prevented it from reacting with the highly hydrophilic alendronate. Accordingly, the choice was made to bind the hydroxybisphosphonate moiety responsible for the bone targeting directly on the squalene chain. Indeed, in 1978 Sekine *et al.* reported that two equivalents of tris (trimethylsilyl)phosphite reacted with acyl chlorides to give the persilylated derivative of 1-hydroxymethylene-1,1-bisphonic acids.[25] Later on, Lecouvey *et al.* enlarged this observation to an efficient one-pot procedure for the synthesis of free 1-hydroxymethylene-1,1-bisphonic acids using tris(trimethylsilyl) phosphite followed by methanolysis of the silyl protecting groups.[26] This process was found also efficient to provide the hydroxybisphosphonic acid derivatives of fatty acids such as lauric and palmitic acids.[27] This approach has now been successfully applied to squalene derivatives in order to obtain a new amphiphilic hydroxybisphosphonate bone targeting moiety (*i.e.*, HbisP–Sq **4**).

Squalenyl-1-hydroxy-1,1-bisphosphonic acid was obtained taking into account the reactivity of tris(trimethylsilyl)phosphite with acid chloride once reported by Sekine *et al.*[25] In the event, treatment of the acid chloride from 1,1′,2-trisnorsqualenic acid **2** with 3 equiv. of tris(trimethylsilyl)phosphite followed by methanol desilylation provided the desired squalene-hydroxybisphosphonic acid **4** in quantitative yield along with an inseparable amount of phosphorous acid.[28] However, long term storage of this material led to substantial degradation of the acid sensitive polyisoprenyl chain. It was finally found that the bis sodium salt **5** obtained in 82% yield upon sodium acetate treatment of the crude hydroxybisphosphonic acid could easily be purified by simple precipitation in methanol. This approach allowed removal of the phosphorous acid by-product, ensuring complete stability for months. However, this salt was very insoluble in both organic and aqueous solvents and was unsuitable for NP formulation using the nanoprecipitation-solvent evaporation technique. Instead, the acid derivative **4** was easily recovered before nanoprecipitation by simple acid treatment with dry hydrochloric acid in methanol (Scheme 1). This compound was fully characterized by IR, ^{1}H, ^{13}C and ^{31}P NMR and mass spectrometry (see SM for further details). The ^{1}H NMR spectrum revealed only the typical lines due to the polyisoprenyl backbone, namely a multiplet around 5.10 ppm assigned to the vinyl protons, a large massif between 2.50 and 1.90 ppm associated with the allylic protons and the 6 methyl group around 1.6 ppm (Figure S1). More informatively, the ^{31}P

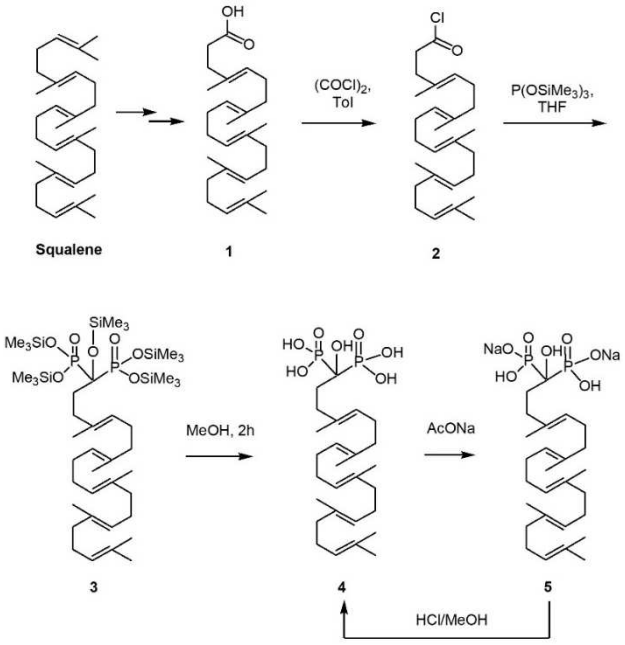

Scheme 1. Schematic representation of the synthesis and purification of HbisP–Sq **4**.

NMR showed a singlet at $\delta = 20.47$ ppm in line with the values previously reported for similar hydroxyl-diphosphonates (Figure S2).[26] ^{13}C NMR spectrum displayed the characteristic triplet at 73.0 ppm with a large $^{2}J_{PC}$ coupling constant corresponding to the quaternary carbon imbedded in the P*C*(OH)P) motive (Figure S3). The IR spectrum is uninformative revealing only three strong bands at 1119, 1023 and 976 cm^{-1} tentatively assigned to the stretching vibration modes of the $PO(OH)_2$ groups (Figure S4).

Design and characterization of the dFdC-Sq | HbisP-Sq NPs

Once the HbisP–Sq was synthetized, squalenoyl nanostructures were prepared using the nanoprecipitation solvent evaporation method as described in the experimental section. Colloidal characterization using dynamic light scattering (DLS) revealed that the acid derivative HbisP–Sq alone was able to form nanostructures with a size between 30 and 120 nm, a heterogeneous or bimodal population distribution (PDI > 0.3) and a strongly negative zeta potential of -66 ± 13 mV (Figure 1ab). dFdC–Sq NPs showed a mean particle size of 113 ± 8 nm, PDI of 0.1 ± 0.01 and a zeta potential of -18 ± 1 mV, in agreement with previous studies.[19] HbisP–Sq NPs and dFdC–Sq NPs were used as controls through all the following experiments. Thereafter, HbisP–Sq and dFdC–Sq were co-nanoprecipitated together to screen a suitable molar ratio of HbisP–Sq *vs* dFdC–Sq (0.005, 0.01, 0.02, 0.05, 0.1 and 1:1, respective ratios were tested, as shown in Figure S5). Interestingly, a very scant amount of HbisP–Sq (molar ratio 0.005:1) in dFdC–Sq triggered drastic decrease of both particle size and zeta potential with respect to dFdC–Sq only NPs (83 nm and −31 mV *vs* 113 nm and −18 mV, respectively). Since bisphosphonates are compounds with a long half-life, remaining irreversibly attached to the bone for months,[29] it was decided to incorporate the lowest amount of HbisP–Sq. Accordingly, the molar ratio 0.01:1 was selected for further experiments, given also that the mean particle size and zeta potential values using higher HbisP–Sq ratios remained similar (70–80 nm and −40-50 mV) but with population heterogeneity values (PDI > 0.2). All in all, the dFdC–Sq | HbisP–Sq NPs at this ratio showed a mean particle size of 75 ± 1 nm, a zeta potential of -43 ± 3 mV and a PDI value of 0.17 ± 0.02. Representative dFdC–Sq and dFdC–Sq | HbisP–Sq nanoformulations merged in Figure 1ab clearly show the differences in size population and zeta potential distribution, attributed to the minimum incorporation of HbisP–Sq in the formulation.

The NPs were also analyzed by Fourier transform infrared spectroscopy (FTIR). IR spectrum in Figure 1c shows the characteristic cytidine IR finger print between the 1000 and 1650 cm^{-1} region associated with the presence of dFdC in dFdC–Sq and dFdC–Sq | HbisP–Sq NPs; the HbisP–Sq NPs sample mainly displayed a broad phosphate signal around 900–1200 cm^{-1}.[30] In this region, it was observed that the C–O stretching of the dFdC–Sq | HbisP–Sq NPs sample was flattened in comparison with that of dFdC–Sq NPs. Thus, the minimal presence of the phosphonic acid groups in the formulation was able to affect and shield the vibrational spectra of dFdC–Sq NPs for wavenumbers near 1075 cm^{-1} presumably through H-bonding interaction,[31] indicating a distinct molecular interaction in the case of the dFdC–Sq | HbisP–Sq NPs. Of note, the corresponding amount of HbisP–Sq alone was not able to input any IR signal.

Colloidal characterization revealed that HbisP–Sq was able to form spontaneously heterogeneous NPs, confirming the amphiphilic chemical structure proposed in the chemistry section. Interestingly, a very small amount of HbisP–Sq was enough to provoke complete remodeling of dFdC–Sq NPs without compromising their population homogeneity. A similar effect was previously reported by adding the amphiphilic compound edelfosine at equimolar concentrations to dFdC–Sq.[32] However, in this study a considerable size and zeta potential reduction was caused by the presence of nanomolar HbisP–Sq concentrations. This could be attributed to the high surface active properties of HbisP–Sq. Moreover, these results suggest that HbisP–Sq molecules might be located onto the NPs surface, dFdC–Sq acting as the core of the NP and drug reservoir. Evidence for this was the zeta potential reduction

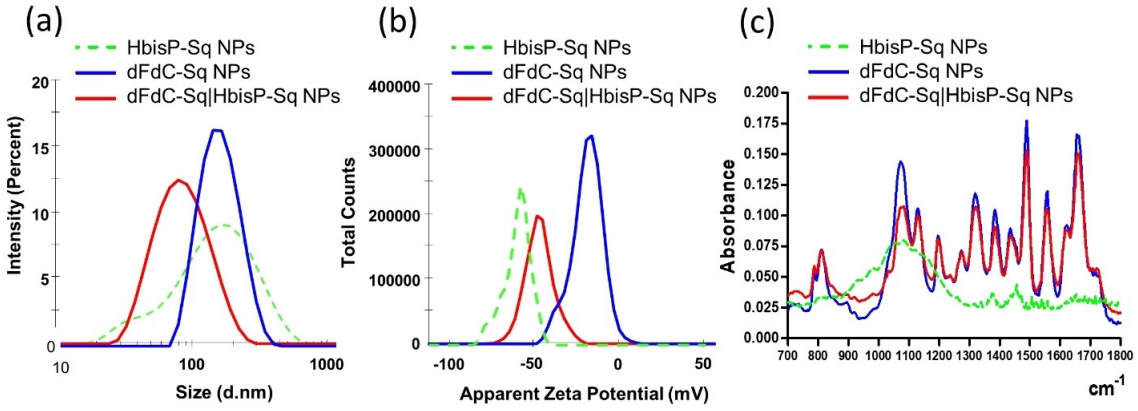

Figure 1. (a) Particle size distribution by intensity, (b) Zeta potential distribution and (c) IR spectra of HbisP–Sq (green dotted line), dFdC–Sq (blue line) and dFdC–Sq | HbisP–Sq NPs at molar ratio 0.01:1 (red line).

observed at the slipping plane of the NP surface, owing exclusively to the presence of the negatively charged phosphate moiety. This was confirmed when the ratio of HbisP–Sq versus dFdC–Sq was augmented in the formulation toward equimolarity (Figure S5b). This was thought to explain also the distinct IR spectra found between dFdC–Sq and dFdC–Sq|HbisP–Sq NPs, assuming that the IR radiation is not penetrating the NPs core.

Morphological analysis

HbisP–Sq, dFdC–Sq and dFdC–Sq|HbisP–Sq nanostructures at the selected ratio were visualized by Transmission electron microscopy (TEM). Samples were negatively stained with phosphotungstic acid to enhance the contrast between the background and the NPs. HbisP–Sq NPs population was very heterogeneous and exhibited a lower particle size (20-60 nm) comparatively to what was observed by DLS (green dotted line, Figure 1a). Although a supramolecular organization was not observed, the larger particles displayed a cup-shaped structure and thus a nano-vesicle appearance (Figure 2a). dFdC–Sq NPs displayed diameters between 80 and 150 nm, in correlation with DLS data (blue line, Figure 1a). TEM images in Figure 2b showed a characteristic inverse hexagonal phase supramolecular structure, in some cases surrounded by an amorphous layer. Interestingly, dFdC–Sq|HbisP–Sq NPs not only presented a reduced mean particle size in agreement with the previous section but also a complete different structural organization/folding and periodicity comparatively to dFdC–Sq NPs. As seen in the Figure 2c, these NPs now displayed an irregular lamellar round shape arranged in concentric multilayers.

dFdC–Sq NPs supramolecular organization has been previously reported by us.[33] However, HbisP–Sq NPs did not present a specific spatial orientation or periodicity. In comparison to DLS, the smaller size of HbisP–Sq NPs as observed in TEM images might be associated with a partial dehydration of the NPs, due to sample drying before TEM analysis. This sometimes entails a particle shrinking and the consequent visualization of cup-shaped structures, a common effect observed with exosomes.[34] This, together with the amphiphilic nature of HbisP–Sq NPs, suggest an unilamelar/bilamellar or vesicular structure. Importantly, TEM. images demonstrated that in dFdC–Sq|HbisP–Sq NPs, HbisP–Sq performed a distinct molecular interaction with dFdC–Sq, leading to a conformational remodeling that resulted in unique helicoidal or concentric multilamellar NPs. These structures are similar to the onion-type dendrimersomes of Zhang *et al.* or the self-assembled fondaparinux NPs prepared by Ralay-Ranaivo *et al.* but with apparently less uniformity between the layers.[35,36] This specific interlamellar spacing may be electrostatically driven by the negatively charged phosphate groups of HbisP–Sq.[37] In that sense, this structure was lost with the equimolecular mixture (ratio 1:1) of dFdC–Sq and HbisP–Sq (Figure S6), indicating that the ratio of HbisP–Sq is crucial for this peculiar assembly to occur.

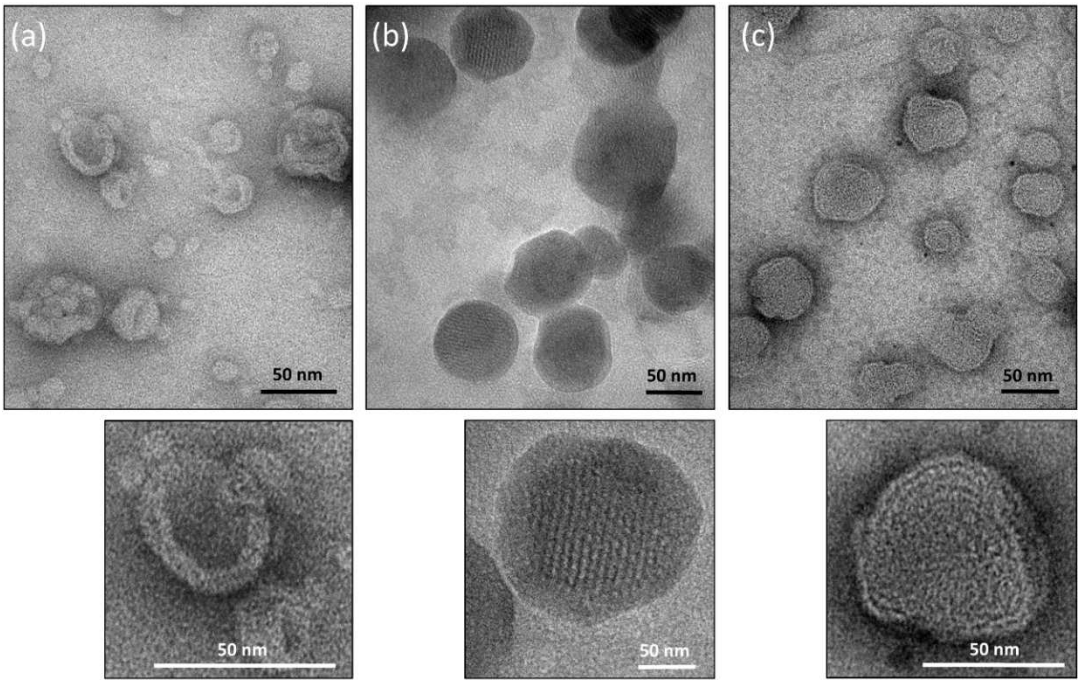

Figure 2. TEM representative micrographs at two magnifications of (a) HbisP–Sq, (b) dFdC–Sq and (c) dFdC–Sq|HbisP–Sq NPs.

HA binding affinity

HA crystals around 25–50 μm were used as an artificial bone substrate for measuring the binding affinity of dFdC–Sq, HbisP–Sq and dFdC–Sq|HbisP–Sq NPs previously loaded with the red fluorescent probe CholEsteryl BODIPY 542/563 (Bchol-red). At different incubation times, HA crystals were pelleted down together with the attached fluorescent nanostructures (see the experimental section for further details). From fluorescence determination in the supernatant, it was observed that the HA binding affinity of both free BChol-red and BChol-red|dFdC–Sq NPs were negligible. On the contrary, BChol-red HbisP–Sq NPs interacted progressively with HA over time, reaching a relative fluorescence value of 45% at 2 hours. BChol-red dFdC–Sq|HbisP–Sq NPs exhibited a slighter binding kinetics progression and reached an indirect fluorescence value of around 10% at 2 hours. After 2 hours incubation, the HA crystals in the pellet were also examined directly by confocal microscopy to confirm previous results. As seen in Figure 3b, HA samples incubated with free BChol-red and BChol-red dFdC–Sq NPs did not present red fluorescence or dye artifacts. Incubation with BChol-red|HbisP–Sq NPs led to a very high HA fluorescence intensity in agreement with the fluorescence data shown in Figure 3a, deduced from fluorescence measurements in the supernatant. Again, HA crystals incubated with BChol-red dFdC–Sq|HbisP–Sq NPs showed significant fluorescence intensity, but lower than after incubation with HbisP–Sq NPs.

An asset of using the red dye fluorescent Bchol-red is that its free counterpart does not give fluorescence *per se* in aqueous media. This allows us to detect any fluorescence intensity variation only if it is correctly encapsulated within the NPs. In that way, BChol-red HbisP–Sq NPs showed a dramatic HA binding affinity and behaved as a positive control in this study. The decoration of dFdC–Sq NPs with HbisP–Sq increased significantly the NPs affinity toward HA in comparison with dFdC–Sq only NPs. Direct visualization of the fluorescent HA crystals by fluorescence microscopy confirmed the kinetic binding assay. Importantly, neither non-specific binding of the control NPs (dFdC–Sq NPs) nor any kind of precipitation of BChol-red was observed. Even if the relative fluorescence value of BChol-red dFdC–Sq|HbisP–Sq NPs, as measured at 2 hours, was 5-fold lower than BChol-red HbisP–Sq NPs (10% *vs* 50%, approximately), it is important to remember that the total amount of HbisP–Sq onto the surface of dFdC–Sq was 100-times lower with the selected ratio 0.01:1. Unfortunately, the incorporation of higher molar ratios of HbisP–Sq did not improve these results, possibly because an excess of HbisP–Sq could be just surfacting the NPs, not being completely integrated or assembled within the dFdC–Sq nanoformulation. In the case of the equimolecular mixture, this could be attributed to loss of NPs structural integrity (Figure S6). Further *in vivo* bone bioaccumulation experiments will elucidate the real potential of this strategy.

In vitro anticancer activity

Preliminary *in vitro* cell proliferative assays were performed using a commercial (U2-OS) and a patient-treated derived (531 M) pediatric OS cell line. Table 1 shows quantitatively the cytotoxic activity of each treatment after 72 h incubation, expressed as the half-maximal inhibitory concentration (IC50). IC50 values for the HbisP–Sq NPs treatment were set at high micromolar concentrations (IC50 > 100 μM) in both cell lines.

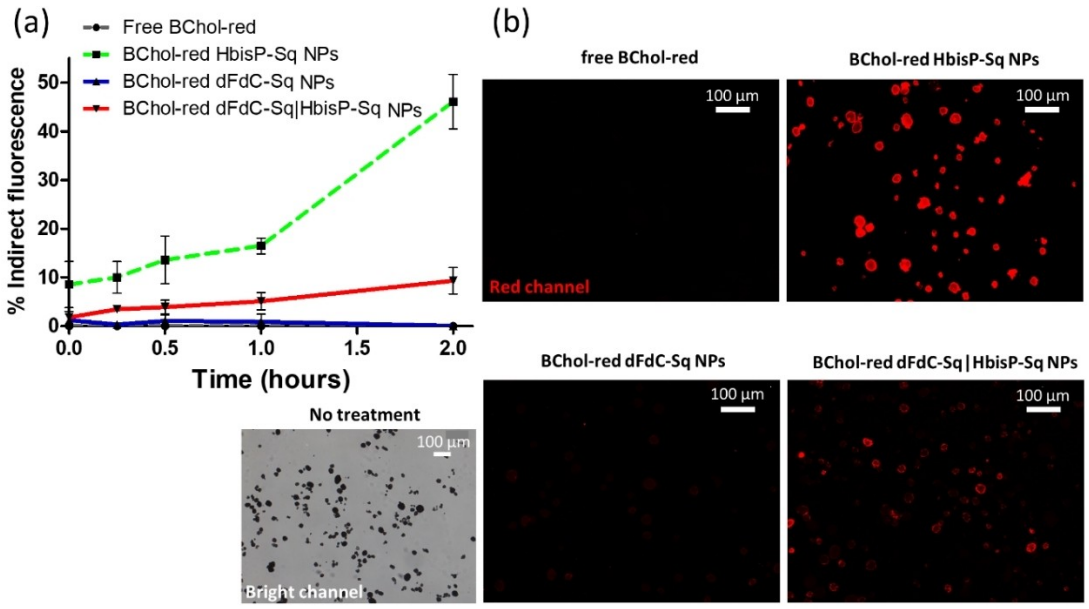

Figure 3. HA binding assays. (a) % relative indirect fluorescence vs time (hours) for free BChol-red, BChol-red HbisP–Sq, BChol-red dFdC–Sq and BChol-red dFdC–Sq|HbisP–Sq NPs (values represent the mean ± s.d., n = 3). (b) Representative red fluorescence and bright channel images of HA crystals after incubation with the nanostructures for 2 hours. Magnification was taken at 10X.

Table 1. *In vitro* anticancer activity in OS cell lines.[a]

OS cell line	dFdC free	HbisP-Sq NPs	dFdC-Sq NPs	dFdC-Sq | HbisP-Sq NPs
U2OS	20 ± 2.5 nM	154 ± 38 μM	205 ± 39 nM	195 ± 43 nM
531 M	17 ± 16 μM	125 ± 14 μM	23 ± 2.9 μM	24 ± 2.6 μM

[a] IC_{50} values (values are the mean ± SD, n = 3).

However, free and squalenoylated dFdC IC50s were nanomolar in the U2-OS cells and micromolar in the 531 M cells. As typically observed, dFdC–Sq NPs displayed higher IC50 *in vitro* values than free dFdC, due to the prodrug nature of dFdC–Sq, reducing the availability of the parent dFdC drug during the incubation time used. Thus, in order to diminish this effect, 72 h incubation times were used instead of 24 h or 48 h. We have previously reported that such difference was not observed *in vivo* since dFdC–Sq NPs avoids rapid dFdC enzymatic metabolization by cytidine deaminase, the amide bond between squalene and dFdC being then intracellularly efficiently cleaved by cathepsin B and D.[19,38] And this explains the better *in vivo* anticancer activity of dFdC NPs, as compared to the drug free. Finally, dFdC–Sq | HbisP–Sq NPs IC50 values (195 ± 43 nM and 24 ± 2.6 μM) were found to be equal to the ones for dFdC–Sq NPs (205 ± 39 nM and 23 ± 2.9 μM) in U2-OS and 531 M cells, respectively.

In the last stretch of this study, we included two pediatric bone tumor cell lines to elucidate if the incorporation of HbisP–Sq had any impact on the anticancer activity of dFdC–Sq NPs. First, HbisP–Sq NPs showed no cytotoxicity that could additively increase the anticancer activity of dFdC–Sq in that concentration range. Cytotoxicity of HbisP–Sq NPs only occurred at high micromolar concentrations in a similar way to the one observed for squalenic acid NPs (*i.e.*, drug-unloaded squalenoyl NPs) in previous studies.[32] This effect might be mainly attributed to cellular membrane solubilization due to the tensioactive properties of HbisP–Sq.[39,40] In this regard, the IC50 values of HbisP–Sq NPs were similar in the commercial U2-OS and the chemoresistant 531 M cells despite their different origins. Importantly, results for both cell lines indicated that the dFdC–Sq particle remodeling triggered by HbisP–Sq was not detrimental to the native anticancer activity of dFdC–Sq NPs. This suggested that any anticancer effect of these NPs is entirely and exclusively attributed to the action of dFdC–Sq, HbisP–Sq acting only as targeting moiety. This may also be optimal with regard to future *in vivo* experiments in terms of toxicity. This strategy is not conceived to limit the maximum tolerated dose of dFdC–Sq NPs due to the presence of another compound in the formulation. The presence of HbisP–Sq is only intended to confer dFdC–Sq NPs with bone retention capacity and therefore achieve better tumor bioaccumulation *in vivo.* This upgrade might ameliorate the therapeutic perspectives not only of free dFdC but also of dFdC–Sq NPs.

Conclusion

Management of aggressive bone tumors still represents a therapeutic conundrum nowadays. The use of precision nanomedicines could ameliorate current treatments by enhancing the action of cytostatic agents through selective targeting to the bone tumor area. With this aim, we successfully synthetized *de novo* an HbisP–Sq with high affinity for calcium ions present in HA. The lipid amphiphilic nature of HbisP–Sq makes this bone targeting moiety suitable for insertion not only into squalenoyl NPs but also in other types of lipid NPs. In our study, insertion of HbisP–Sq within dFdC–Sq led to the formation of multilamellar monodisperse dFdC–Sq | HbisP–Sq NPs of 75 nm size with bone binding affinity skills. The drug loading of this formulation was very high given that it was exclusively made by drugs without additional polymers or other lipid carrier materials. dFdC–Sq NPs rearrangement triggered by HbisP–Sq was not associated with any *in vitro* lessening of anticancer efficacy. This suggests that this approach should be further evaluated in experimental OS murine tumor models. The expected advantage rely on: (i) dFdC half-life enhancement via squalenoylation and; (ii) improved NP bone retention by means of HbisP–Sq decoration. In case of success, dFdC–Sq | HbisP–Sq NPs could also decrease chemotherapy-associated toxicity and improve the quality of life of OS high-risk patients.

Experimental Section

Chemistry

Chemicals obtained from commercial suppliers were used without further purification. Squalene, tris(trimethylsilyl)phosphite and 3 M HCl in methanol was purchased from Sigma-Aldrich Chemical Co., France. IR spectra were obtained as solid or neat liquid on a Fourier Transform Bruker Vector 22 spectrometer. Only significant absorptions are listed. The ^{1}H and ^{13}C NMR spectra were recorded on Bruker Avance 300 (300 MHz and 75 MHz, for ^{1}H and ^{13}C, respectively). Recognition of methyl, methylene, methine, and quaternary carbon nuclei in ^{13}C NMR spectra rests on the J-modulated spin-echo sequence. The ^{31}P NMR spectra were recorded on Bruker AC 200 P (81 MHz). Mass spectra were recorded on a Bruker Esquire-LC. Analytical thin-layer chromatography was performed on Merck silica gel 60F254 glass precoated plates (0.25 mm layer). Column chromatography was performed on Merck silica gel 60 (230–400 mesh ASTM). Tetrahydrofuran (THF) was distilled from sodium/benzophenone ketyl. Methanol was dried over magnesium and distilled. Toluene was distilled from calcium hydride, under a nitrogen atmosphere. All reactions involving air- or water-sensitive compounds were routinely conducted in glassware which was flame-dried under a positive pressure of nitrogen or argon.

4,8,13,17,21-Pentamethyl-docosa-4,8,12,16,20-pentaenoyl chloride (2). A solution of trisnorsqualenic acid[24] (1.80, 4.5 mmol) in anhydrous toluene (10 mL) was degassed by bubbling a stream of nitrogen through the solution for 5 min. Oxalyl chloride (1.74 g, 13.8 mmol) was added dropwise at 20 °C. The reaction mixture was stirred for 3 h at the same temperature and concentrated under reduced pressure to give the title compound as a pale yellow oil which is used directly in the next step. IR (film) ν: 2920, 1799, 1443, 1382, 955, 893 cm^{-1}; ^{1}H NMR (300 MHz, $CDCl_3$) δ : 5.23-5.10 (m, 5 H, =*CH*), 2.45 (t, J = 7.3 Hz, 2 H, CH_2COCl), 2.30 (t, J = 7.5 Hz, 2H,

CH_2CH_2COCl), 2.15-1.95 (m, 16 H), 1.70 (s, 3H, CH_3, C=C(CH_3)$_2$), 1.62 (s, 15H, CH_3, =C(CH_3)$_2$$CH_2$) ppm; ^{13}C NMR (75 MHz, $CDCl_3$), δ :173.2 (C, COCl), 135.1 (C, C=CH), 134.8 (C, C=CH), 134.6 (C, C=CH), 131.4 (C, C=CH), 131.1 (C, C=CH), 126.6 (CH, C=CH), 124.7 (CH, C=CH), 124.4 (CH, C=CH), 124.3 (2CH, C=CH), 45.8 (CH_2), 39.7 ($2CH_2$), 34.4 (CH_2), 34.6 (CH_2), 28.2 ($2CH_2$), 26.8 (CH_2), 26.7 (CH_2), 26.5 (CH_2), 25.7 (CH_3, C=C(CH_3)$_2$), 17.6 (CH_3), 16.0 (CH_3), 15.9 (2 CH_3), 15.8 (CH_3) ppm.

Ditrimethylsilyl [(4*E*,8*E*,12*E*,16*E*)-1-{bis[(trimethylsilyl)oxy] phosphoryl}-4,8,13,17,21-pentamethyl-1-[(trimethylsilyl)oxy]docosa-4,8,12,16,20-pentaen-1-yl]phosphonate (3). In a flame-dried 50 mL round bottom flask under argon was introduced squalenoyl chloride 2 (289 mg, 0.69 mmol, 1 equiv.) in THF (1.2 mL). Then, tris (trimethylsilyl)phosphite (621 mg, 2.08 mmol, 3 equiv.) was added dropwise at 0 °C. Once the addition was complete, the reaction mixture was stirred at room temperature for 1 h. Volatile fractions were then evaporated under reduced pressure (1 mbar) to leave a colorless oil (630 mg, quant), which was used directly in the next step. ^{1}H NMR (300 MHz, C_6D_6) δ: 5.43 (t, J=6.4 Hz, 1H, HC=), 5.40-5.15 (m, 4H, HC=), 2.65-2.00 (m, 20H), 1.74 (s, 3H, C=C(CH_3)), 1.67 (s, 3H, =C(CH_3)$_2$$CH_2$), 1.61 (s, 3H, =C($CH_3$)$_2$$CH_2$), 1.60 (s, 6H, =C($CH_3$)$_2$$CH_2$), 1.51 (s, 3H, =C($CH_3$)$_2$$CH_2$), 0.42 (s, 18H, Si$CH_3$), 0.38 (s, 18H, Si$CH_3$), 0.16 (s, 9H, Si$CH_3$) ppm; ^{31}P NMR (81 MHz, C_6D_6) δ: 2.49 (s) ppm.

[(4*E*,8*E*,12*E*,16*E*)-1-Hydroxy-4,8,13,17,21-pentamethyl-1-phosphono-docosa-4,8,12,16,20-pentaen-1-yl]phosphonic acid disodium salt (5). The oil obtained above (630 mg, 0.69 mmol) was treated with methanol (10 mL) at room temperature for 4 hours. Removal of the solvent under reduced pressure at 20 °C yielded a viscous oil which was taken into methanol (10 mL). A solution of sodium acetate (114 mg, 1.39 mmol) in methanol (5 mL) was added dropwise. A voluminous white precipitate was immediately formed. The mixture was centrifuged (6,000 rpm) and the supernatant decanted. The precipitate was collected, washed with water and dried under vacuum to give the title compound (351 mg, 86% yield) as a white solid. This highly insoluble material can be conveniently stored for months. Mp >230 °C; IR (neat,) ν: 2979, 2965, 2924, 2911, 2855, 1658, 1448, 1383, 1241, 1176 (s), 1152, 1060 (s), 926 (s), 850, 748, 675, 658 cm^{-1}; MS (ESI-) *m/z* (%) 545.2 (100) [M-2Na+H]$^-$; 465.3 (35) [M-PO_3Na_2].

[(4*E*,8*E*,12*E*,16*E*)-1-Hydroxy-4,8,13,17,21-pentamethyl-1-phospho-nodocosa-4,8,12,16,20-pentaen-1-yl]phosphonic acid (4). A suspension of the sodium salt **(5)** (200 mg, 0.34 mmol) in methanol (5 mL) was treated with 3 M HCl in methanol (0.25 mL, 0.68 mmol) for few minutes until the solid was completely dissolved. The solvent was quickly removed under reduced pressure at room temperature to leave a colorless thick oil (185 mg, quantitative) which was used rapidly for the nanoprecipitation step. IR (neat,) ν: 3455–2800, 2944, 2915, 2830, 2600–2400, 1663, 1456, 1383, 1118, 1023 (s), 1012 (s), 976, 933, 871; ^{1}H NMR (300 MHz, CD_3OD) δ: 5.21 (t, J=5.4 Hz, 1H, HC=), 5.20-5.05 (m, 4H, HC=), 2.40-2.31 (m, 2H), 2.20-1.90 (18 H), 1.66 (s, 3H, CH_3), 1.64 (s, 3H, CH_3), 1.60 (s, 3H, CH_3), 1.59 (s, 9H, CH_3) ppm; ^{13}C NMR (75 MHz, CD_3OD), δ : 135.0 (C, C=CH), 134.7 (C, C=CH), 134.6 (C, C=CH), 134.2 (C, C=CH), 130.6 (C, C=CH), 124.2 (CH, C=CH), 124.1 (4CH, C=CH), 73.0 (C, t, J_{CP}= 145.9 Hz, PC(OH)P), 48.5 (CH_2), 39.4 ($2CH_2$), 33.1 (t, J_{CP}=5.7 Hz, CH_2), 32.7 (CH_2), 27.9 ($2CH_2$), 26.6 (CH_2), 26.4 (CH_2), 26.2 (CH_2), 24.5 (CH_3, C=C(CH_3)$_2$), 16.5 (CH_3, =C(CH_3)$_2$$CH_2$), 14.9 ($CH_3$, =C($CH_3$)$_2$$CH_2$), 14.8 (3$CH_3$, =C($CH_3$)$_2$$CH_2$) ppm; ^{31}P NMR (81 MHz, CD_3OD) δ: 20.47 (s) ppm; MS (ESI-) *m/z*(%) 581.3 (10%) [M+Cl]$^-$, 545.4 (100) [M–H]$^-$, 272.3 (45) [M-2H]$^{2-}$.

Preparation and characterization of the nanostructures

The synthesis of dFdC–Sq was performed as previously described.[19,33] Ethanol absolute was purchased from Panreac Química (Barcelona, Spain). Phosphotungstic acid hydrate and HA synthetic powder were purchased from Sigma Aldrich (Barcelona, Spain). BChol-red was purchased from Thermo Fisher Scientific (Massachusetts, USA).

Squalenoyl NPs were formulated using the nanoprecipitation-solvent evaporation method. dFdC–Sq or HbisP–Sq alone or mixed and previously dissolved in 200 μL of ethanol were added dropwise under stirring into 2 mL of distilled water. Ethanol was then evaporated using a Rotavapor (Buchi R-210/215, Buchi Corp., Canada) to obtain an aqueous nanosuspension of HbisP–Sq, dFdC–Sq, or dFdC–Sq|HbisP–Sq at a final concentration of 1.16 μmol.mL^{-1}. Fluorescent NPs were prepared employing the same procedure by incorporating in the ethanol solution the orange-red dye BChol-red (2% w/w).

Mean particle size (Z-average) and polydispersity index (PDI) of the NPs were determined at 25 °C by DLS (Zetasizer Nano ZS Malvern; Malvern Instruments SA, UK) after 1:20 dilution in ultrapure water. Surface charge of the NPs was characterized by measuring the zeta potential with laser Doppler velocimetry (Zetasizer Nano ZS Malvern; Malvern Instruments SA, UK) and using the Smoluchowski equation ($n \geq 3$).

Fourier transform infrared analysis. Infrared absorbance of the NPs was analyzed with an IR (FTIR) spectrometer IRAffinity-1S (Shimadzu, Duisburg, Germany). Briefly, the aqueous nanosuspensions were dropped in an ATR Golden-GateTM top-plate set at 70 °C for a fast water evaporation. Scan runs value was set at 32 with a resolution of 4 cm^{-1} and Happ-Genzel apodization.

Electron microscopy imaging. The morphology of the squalenoyl NPs was characterized by TEM using a negative staining agent. Electron microscopy images were recorded on a T20-FEI Tecnai thermoionic microscope operated at an acceleration voltage of 200 kV. Samples were prepared by dropping 20 μL of the aqueous nanosuspensions in carbon coated copper grids (200 mesh), dried at room temperature and stained with a negative staining agent (phosphotungstic acid).

Hydroxyapatite binding assays. Practically, fluorescent HbisP–Sq NPs, dFdC–Sq, and dFdC–Sq|HbisP–Sq NPs at a concentration of 375 μg mL^{-1} were incubated with 5 mg of HA crystals in a total volume of 0.5 mL of distilled water for different periods of time (0, 15, 30, 60 and 120 min) at 37 °C. Considering that the NPs are not pelleted down under mild centrifugation, samples were smoothly centrifuged at 2,000 rpm for 2 min to spin down HA crystals together with the NPs bound to them. This methodology was adapted from the one previously described by Nguyen *et al.*[41] Finally, 100 μL of supernatants were measured in triplicate wells using a Tecan GENios microplate fluorescence reader (Tecan Group Ltd, Maennedorf, Switzerland) at an excitation and emission respective wavelength of 540 and 580 nm ($n \geq 3$). The binding affinity (%) of the fluorescent NPs to HA ($Ca_5(PO_4)_3(OH)$) was calculated indirectly by measuring the fluorescence intensity of the supernatants with respect to the initial fluorescence intensity of the treatments without HA by using the formula below.

$$\textit{Binding affinity}\ (\%) = \left(\frac{F-f}{F}\right) \times 100$$

F: initial fluorescence intensity value of the fluorescent NPs

f: fluorescence intensity value of the fluorescent NPs after incubation with HA

After supernatant removal, the pelleted fluorescent HA crystals were visualized by fluorescence microscopy after 120 min incubation with the fluorescent nanostructures. Fluorescent HA crystal samples were mounted in microscopy slides and imaged with a LSM 800 confocal fluorescence microscope (Zeiss, Madrid, Spain). Excitation wavelength was set at 543 nm and red-fluorescent detection was performed through a 560 nm filter.

Biology

Celltiter 96® aqueous one solution cell proliferation assay (MTS) was purchased from Promega (Alcobendas, Spain). Heat inactivated fetal bovine serum, Trypsin-EDTA, penicillin/streptomycin and alpha-MEM cell medium were purchased from Gibco® (Invitrogen Inc., Carlsbad, USA). Phosphate Buffer Saline (PBS) and McCoy's 5 A cell medium were provided by Lonza (Verviers, Belgium). Tissue cell culture 96-well plate was purchased from Corning Inc. (New York, USA). Gemcitabine (2′,2′-difluorodeoxycytidine) hydrochloride was purchased from Carbosynth, Ltd. (Compton, UK). The human immortalized OS cell line U-2 OS (ATCC®HTB96™) was acquired from the American Type Culture Collection (Sigma–Aldrich). A metastatic pediatric OS cell line termed 531 M was obtained from a patient treated at the Clínica Universidad de Navarra (Pamplona, Spain) with a protocol approved by the local ethics committee.[42] U-2 OS and 531 M cell lines were cultured in McCoy's 5 A and MEM-alpha cell mediums respectively, supplemented with 10% of heat inactivated fetal bovine serum and 1% penicillin/streptomycin and incubated in a humidified 5% carbon dioxide atmosphere at 37 °C.

In vitro proliferative studies. For the *in vitro* cytotoxicity assays, U-2 OS and 531 M cells were seeded on 96-well plates at a density of respectively 2,000 and 10,000 cells per 100 μL/well, 24 h before the addition of cell medium dilutions of free dFdC, HbisP–Sq NPs, dFdC–Sq or dFdC–Sq|HbisP–Sq NPs in triplicate wells. After 72 h incubation, the treatment medium of each well was replaced by complete cell medium containing 15% v/v of MTS. Absorbance was measured 3 h later in a microplate reader (iEMS reader MF, Labsystem, Helsinki, Finland) at a test wavelength of 492 nm and 690 nm for the reference wavelength. The concentration of drug required to inhibit cell proliferation by 50% (IC50) was calculated using GraphPad Prism version 5.0 (GraphPad Software, San Diego, CA, USA) ($n \geq 3$).

Acknowledgements

Asociación Española Contra el Cáncer (AECC) (CI14142069BLAN), Fundación Caja Navarra/Obra Social La Caixa and the Asociación de familiares y amigos de pacientes con neuroblastoma (NEN, Nico contra el cáncer) are gratefully acknowledged. CIBER-BBN is an initiative funded by the VI Spanish National R&D&i Plan 2008–2011, Iniciativa Ingenio 2010, Consolider Program, CIBER Actions and financed by the Instituto de Salud Carlos III (Spain) with assistance from the European Regional Development Fund.

Conflict of Interest

The authors declare no conflict of interest.

Keywords: osteosarcoma · antitumor agents · hydroxyapatite · bisphosphonates · nanoparticles

[1] B. Kasper, P. Hohenberger, *Crit. Rev. Oncol. Hematol.* **2020**, *155*: 103108.
[2] M. Bergovec, O. Kubat, M. Smerdelj, S. Seiwerth, A. Bonevski, D. Orlic, *Cancer Epidemiol.* **2015**, *39*, 298–302.
[3] S. S. Bielack, S. Hecker-Nolting, C. Blattmann, L. Kager, *F1000Research* **2016**, *5*: 2767.
[4] N. J. Croteau, T. E. Heaton, *Children* **2019**, *6*, 6.
[5] L. Kager, G. Tamamyan, S. Bielack, *Futur. Oncol.* **2017**, *13*, 357–368.
[6] M. S. Isakoff, S. S. Bielack, P. Meltzer, R. Gorlick, *J. Clin. Oncol.* **2015**, *33*, 3029–3035.
[7] C. Rodríguez-Nogales, Y. González-Fernández, A. Aldaz, P. Couvreur, M. J. Blanco-Prieto, *ACS Nano* **2018**, *12*, 7482–7496.
[8] J. Shi, P. W. Kantoff, R. Wooster, O. C. Farokhzad, *Nat. Rev. Cancer* **2016**, *17*, 20–37.
[9] L. Salvioni, M. A. Rizzuto, J. A. Bertolini, L. Pandolfi, M. Colombo, D. Prosperi, *Cancers (Basel).* **2019**, *11*, 1855.
[10] A. C. Anselmo, S. Mitragotri, *Bioeng. Transl. Med.* **2019**, *4*, e10143.
[11] H. Maeda, J. Wu, T. Sawa, Y. Matsumura, K. Hori, *J. Controlled Release* **2000**, *65*, 271–84.
[12] N. Bertrand, J. Wu, X. Xu, N. Kamaly, O. C. Farokhzad, *Adv. Drug Delivery Rev.* **2014**, *66*, 2–25.
[13] R. N. Young, M. D. Grynpas, *Curr. Opin. Pharmacol.* **2018**, *40*, 87–94.
[14] S. A. Low, J. Kopeček, *Adv. Drug Delivery Rev.* **2012**, *64*, 1189–204.
[15] N. R. Fuggle, B. Curtis, M. Clynes, J. Zhang, K. Ward, M. K. Javaid, N. C. Harvey, E. Dennison, C. Cooper, *Bone* **2020**, 115833.
[16] Z. A. Habib, *Expert Rev. Endocrinol. Metab.* **2017**, *12*, 59–71.
[17] F. Ordikhani, N. Zandi, M. Mazaheri, G. A. Luther, M. Ghovvati, A. Akbarzadeh, N. Annabi, *Med. Res. Rev.* **2020**, 41, 1221–1254.
[18] X. Gao, L. Li, X. Cai, Q. Huang, J. Xiao, Y. Cheng, *Biomaterials* **2021**, *265:*120404.
[19] P. Couvreur, B. Stella, L. Harivardhan Reddy, H. Hillaireau, C. Dubernet, D. Desmaëie, S. Lepêtre-Mouelhi, F. Rocco, N. Dereuddre-Bosquet, P. Clayette, V. Rosilio, V. Marsaud, J. M. Renoir, L. Cattel, *Nano Lett.* **2006**, *6*, 2544–2548.
[20] D. Desmaële, R. Gref, P. Couvreur, *J. Controlled Release* **2012**, *161*, 609–618.
[21] L. H. Reddy, P.-E. Marque, C. Dubernet, S.-L. Mouelhi, D. Desmaele, P. Couvreur, *J. Pharmacol. Exp. Ther.* **2008**, *325*, 484–490.
[22] S. Réjiba, L. H. Reddy, C. Bigand, C. Parmentier, P. Couvreur, A. Hajri, *Nanomedicine Nanotechnology, Biol. Med.* **2011**, *7*, 841–849.
[23] T. L. Lu, H. J. Hu, W. Zhao, T. Chen, *Drug Dev. Ind. Pharm.* **2011**, *37*, 656–663.
[24] E. E. van Tamelen, T. J. Curphey, *Tetrahedron Lett.* **1962**, *3*, 121–124.
[25] M. Sekine, T. Hata, *J. Chem. Soc. Chem. Commun.* **1978**, 285b – 286.
[26] M. Lecouvey, I. Mallard, T. Bailly, R. Burgada, Y. Leroux, *Tetrahedron Lett.* **2001**, *42*, 8475–8478.
[27] M. A. Didi, A. Elias, D. Villemin, *Solvent Extr. Ion Exch.* **2002**, *20*, 505–513.
[28] M. Egorov, S. Aoun, M. Padrines, F. Redini, D. Heymann, J. Lebreton, M. Mathé-Allainmat, *Eur. J. Org. Chem.* **2011**, *2011*, 7148–7154.
[29] S. Cremers, F. (Hal) Ebetino, R. Phipps, *Bone* **2020**, *139*, 115501.
[30] J. R. Bezerra Neto, P. de Lima Neto, F. A. M. Sales, E. E. da Silva, L. O. Ladeira, V. N. Freire, E. W. S. Caetano, *J. Raman Spectrosc.* **2014**, *45*, 801–806.
[31] M. K. Ahmed, S. Ali, E. Wojcik, *Spectrosc. Lett.* **2012**, *45*, 420–423.
[32] C. Rodríguez-Nogales, V. Sebastián, S. Irusta, D. Desmaële, P. Couvreur, M. J. Blanco-Prieto, *Eur. J. Pharm. Biopharm.* **2019**, *144*, 165–173.
[33] P. Couvreur, L. H. Reddy, S. Mangenot, J. H. Poupaert, D. Desmaële, S. Lepêtre-Mouelhi, B. Pili, C. Bourgaux, H. Amenitsch, M. Ollivon, *Small* **2008**, *4*, 247–253.
[34] V. S. Chernyshev, R. Rachamadugu, Y. H. Tseng, D. M. Belnap, Y. Jia, K. J. Branch, A. E. Butterfield, L. F. Pease, P. S. Bernard, M. Skliar, *Anal. Bioanal. Chem.* **2015**, *407*, 3285–3301.
[35] S. Zhang, H. J. Sun, A. D. Hughes, R. O. Moussodia, A. Bertin, Y. Chen, D. J. Pochan, P. A. Heiney, M. L. Klein, V. Percec, *Proc. Natl. Acad. Sci. USA* **2014**, *111*, 9058–9063.
[36] B. Ralay-Ranaivo, D. Desmaële, E. P. Bianchini, E. Lepeltier, C. Bourgaux, D. Borgel, T. Pouget, J. F. Tranchant, P. Couvreur, R. Gref, *J. Controlled Release* **2014**, *194*, 323–331.
[37] S. Julin, Nonappa, B. Shen, V. Linko, M. A. Kostiainen, *Angew. Chem. Int. Ed.* **2020**, *60*, 827–833.

[38] L. H. Reddy, H. Khoury, A. Paci, A. Deroussent, H. Ferreira, C. Dubernet, X. Declèves, M. Besnard, H. Chacun, S. Lepêtre-Mouelhi, D. Desmaële, B. Rousseau, C. Laugier, J.-C. Cintrat, G. Vassal, P. Couvreur, *Drug Metab. Dispos.* **2008**, *36*, 1570–7.
[39] B. Arechabala, C. Coiffard, P. Rivalland, L. J. M. Coiffard, Y. De Roeck-Holtzhauer, *J. Appl. Toxicol.* **1999**, *19*, 163–165.
[40] S. Przestalski, J. Sarapuk, H. Kleszczyńska, J. Gabrielska, J. Hładyszowski, Z. Trela, J. Kuczera, *Acta Biochim. Pol.* **2000**, *47*, 627–638.
[41] T. D. T. Nguyen, A. Pitchaimani, S. Aryal, *Sci. Rep.* **2016**, *6*:36707.
[42] A. Patiño-García, M. Zalacain, C. Folio, C. Zandueta, L. Sierrasesúmaga, M. San Julián, G. Toledo, J. De Las Rivas, F. Lecanda, *Clin. Cancer Res.* **2009**, *15*, 5082–509.

Manuscript received: June 30, 2021
Revised manuscript received: August 30, 2021
Accepted manuscript online: September 28, 2021
Version of record online: October 22, 2021